

Observation of quantum domain melting and its simulation with a quantum computer

Jaka Vodeb^{1,2}, Michele Diego¹, Yevhenii Vaskivskyi¹, Yaroslav Gerasimenko¹, Viktor Kabanov¹ and Dragan Mihailovic^{1,2,3}

¹*Jozef Stefan Institute, Jamova 39, 1000 Ljubljana, Slovenia*

²*Faculty of Mathematics and Physics, University of Ljubljana, Jadranska 19, Ljubljana, Slovenia*

³*CENN Nanocenter, Jamova 39, 1000 Ljubljana, Slovenia*

Domains are homogeneous areas of discrete symmetry, created in nonequilibrium phase transitions. They are separated by domain walls, topological objects which prevent them from fusing together. Domains may reconfigure by thermally-driven microscopic processes^{1,2}, and in quantum systems, by macroscopic quantum tunnelling (MQT). The underlying microscopic physics that defines the system's energy landscape for tunnelling is of interest in many different systems, from cosmology^{3–5} and other quantum domain systems⁶, and more generally to nuclear physics, matter waves⁷, magnetism^{7–9}, and biology¹⁰. A unique opportunity to investigate the dynamics of microscopic correlations leading to emergent behaviour, such as quantum domain dynamics is offered by quantum materials. Here, as a direct realization of Feynman's idea of using a quantum computer to simulate a quantum system¹¹, we report an investigation of quantum electron reconfiguration dynamics and domain melting in two matching embodiments: a prototypical two-dimensionally electronically ordered solid-state quantum material, and a simulation on a latest generation quantum simulator¹². We use scanning tunnelling microscopy to measure the time-evolution of electronic domain reconfiguration dynamics, and compare this with the time evolution of domains in an ensemble of entangled correlated electrons in simulated quantum domain melting. The domain reconfiguration is found to proceed by tunnelling in an emergent, self-configuring energy landscape, with characteristic step-like time evolution and temperature- dependences observed macroscopically. The remarkable correspondence in the dynamics of a quantum material and a quantum simulation opens the way to understanding of emergent behaviour in diverse interacting many-body quantum systems at the microscopic level.

Temporally evolving systems undergoing rapid phase transitions generate copious spatial inhomogeneities in the form of domains whose classical relaxation dynamics is universally followed. For example, in first order phase transitions, initial nucleation of an emerging phase is typically followed by coalescence¹ and eventually by the growth of larger domains at the expense of smaller ones by ‘ripening’². The classical kinetics is diffusion-driven, and leads to power-law temporal evolution of the domain radius, $r(t) \sim t^n$, where $n = \frac{1}{2}$ for nucleation, changing to $n = \frac{1}{3}$ for coalescence, and eventually to a slow double-exponential ripening processes². These models don’t apply in quantum systems¹³, where we may expect to observe tunneling between different domain configurations. MQT processes can occur on a wide variety of timescales, ranging from $\sim 10^{10\sim 30}$ years for the universe³, from 10^{-14} to 14 seconds for alpha particle decay in different isotopes of Be¹⁴, and \sim microseconds in quantum vortex creep phenomena¹⁵ and macroscopic matter waves¹⁶. To investigate the underlying microscopic quantum dynamics that defines the emergent phenomena in such systems, the microscopic quantum system dynamics needs to be experimentally observable in detail. An excellent model system for investigating quantum domain dynamics turn out to be electronically ordered layered transition metal dichalcogenides (TMDs). These materials’ generic properties may be abstracted to a triangular 2-dimensional lattice, sparsely filled with electrons that order into an electronic crystal (Fig. 1a)^{17,18}. The electronically ordered state is stabilized by correlations and the electron-phonon interaction. The electrons can be considered as dressed quasiparticles – polarons - arranged in a sparse commensurate lattice¹⁷. The underlying triangular crystal lattice geometrically constrains the regular filling patterns to ‘magic’ filling fractions $\frac{1}{3}, \frac{1}{7}, \frac{1}{9}, \frac{1}{13}, \dots$, which in turn define the commensurate electronic states that are favored in natural materials³. Departure from magic fractions can be induced by chemical doping, strain, or other external stimuli, such as photodoping^{19,20} or carrier injection²¹⁻²³, which introduce domain walls that can accommodate additional electrons (or holes) in the electronic lattice (Fig. 1b). Such domain walls arising from electron ‘overcrowding’ have been observed in numerous TMDs¹⁷ and are associated with the appearance of superconductivity²⁴, but 1T-TaS₂ is of special interest because the domain reconfiguration dynamics can be studied on an experimentally accessible timescale²⁰. The domain state in 1T-TaS₂ can be considered as an emergent many-body state, formed on the basis of microscopic interactions between the electrons, which makes it amenable to a microscopic theoretical formulation of the domain dynamics problem. Additional interest in the dynamics of the domain state in 1T-TaS₂ comes from the possibility of using domain reconfiguration as a basis for a low-temperature memory device²³, where quantum domain melting processes may functionally determine the long-term data retention. The experimental motivation for the present work comes from our observation, by scanning tunneling microscopy (STM), of temperature-independent, tip-independent

reconfiguration of domains at low temperature which cannot be explained by classical thermally assisted processes²⁵. A theoretical WKB estimate presented in the supplement (SI) confirms that tunneling between domain configurations is plausible on timescales accessible by STM.

A domain state in 1T-TaS₂ can be conveniently set up by an electrical pulse through an STM tip at 4 K^{21,22,25}. As the domain structure evolves in time, its configuration is recorded periodically by STM (Fig. 1c), which amounts to a classical ‘snapshot’ of the system. The motion of individual electrons in between measurements is quantified by comparing sequential images (Fig. 1c), and counting the total number of electrons that moved ΔN , and expressed as the fraction of electrons moved $f = \frac{\Delta N}{N}$, where N is the total number of electrons per frame (Fig. 1d). Typically, on the same spot on the sample, large pseudo-random jumps appear with time (Fig. 1e), reflecting the discrete nature of domain reconfiguration²⁰. $f(t)$ averaged over a large number of scans on different areas of the sample at 5 K appears close to an exponential decay, but is inconsistent with expected classical power law time dependences $f(t) \sim r(t)^2 \sim t^{-1}$ or $t^{-2/3}$, characteristic of nucleation or coalescence processes¹ respectively, observed at higher temperature²⁶ (see Fig. 1g). An energy landscape plotted in terms of in-plane configurational coordinates q_1 and q_2 suggests the paths of both thermally activated, and tunneling processes between configurational states (insert to Fig. 1f).

A number of experiments designed to test STM tip-current dependence of the reconfiguration process are performed. Comparing $f(t)$ obtained by scanning at regular intervals (Fig. 1g), with $f(t)$ measured under identical experimental conditions but with *no* tip scanning (Fig. 1h) shows very similar exponential decay constants of $\tau = 1040 \pm 90$ s and 945 ± 80 s respectively. In another test, increasing the tip current and voltage to the extent that the deposited Joule heating is increased 1000-fold, we find that the relaxation increases less than two-fold (see SI for details). We conclude that the tip current has a relatively small effect on domain reconfiguration rate, and the main recombination processes are not induced by the tip.

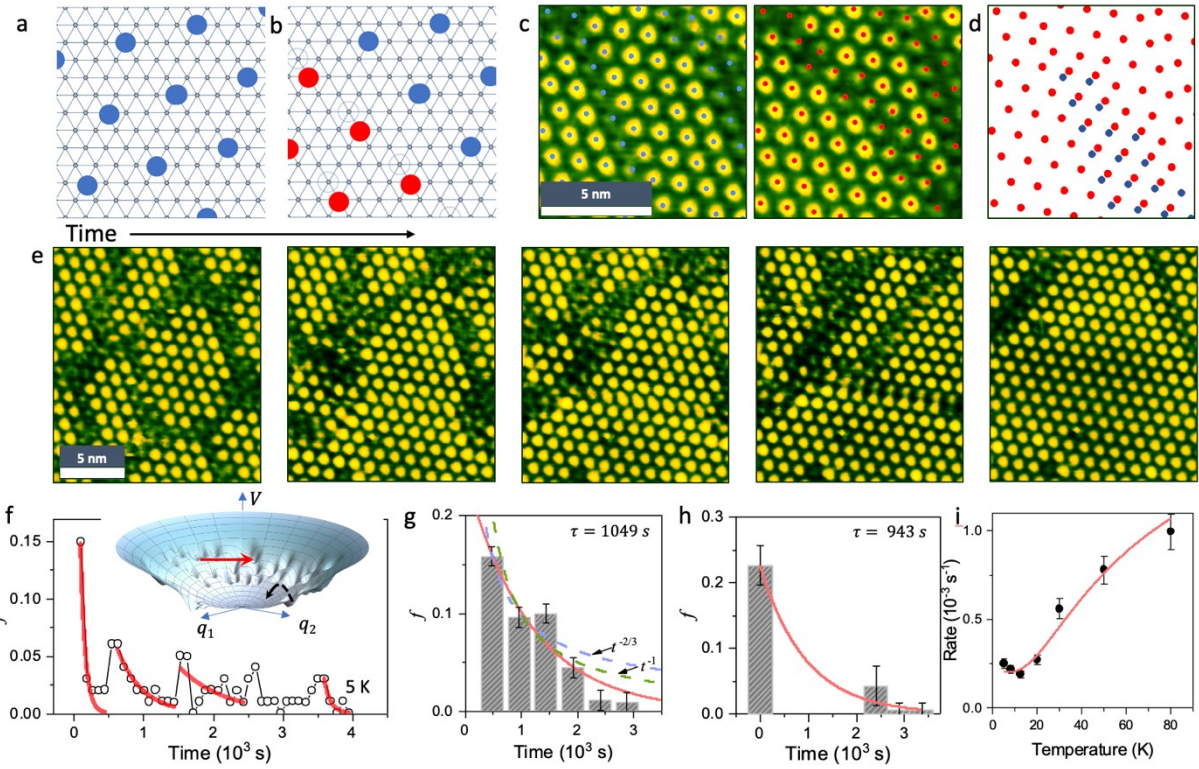


Figure 1. The Ta lattice in 1T-TaS₂ (small circles) showing occupied localized electron sites (blue and orange circles) a) in the ground state, and b) near a domain wall. c) A time series STM measurement showing domain melting. (Tip parameters: -0.8 V, 50 pA). d) Two consecutive STM measurements, and the corresponding polaron displacements (blue and orange circles correspond to the two measurements). e) A series of STM images showing domain reconfiguration at 8 minute intervals. f) The fraction of electrons moved $f(t)$ as a function of time on the same sample spot at 5 K. The jumps correspond to big (observable) configurational changes that cause concurrent changes in the reconfiguration barrier as the energy landscape changes (shown in f). Red lines correspond to exponential fits. g) $f(t)$ averaged over different areas of the sample, with periodic STM scans. Exponential and power law fits to the data are shown (solid and dashed lines respectively). The exponents are indicated. Error bars correspond to errors in counting. h) Same as F, except with a 32-minute gap in scanning the first point. The exponential fit (red line) are shown. i) The temperature dependence of R averaged over a large number of decays.

The temperature dependence of the reconfiguration rate is shown in Fig. 1i. At low T, the rate is approximately constant to ~ 20 K, but increases with T and begins to saturate above ~ 60 K. The data are fit to a generic phenomenological model²⁷ commonly used for transport in disordered systems: $R(T) = R_q + R_0 \exp\left(-\frac{E_B}{k_B T}\right)$. $R_q \simeq 2.2 \pm 0.2 \times 10^{-4} \text{ s}^{-1}$ is the temperature-independent quantum tunneling rate, while the second term describes temperature-activated hopping across a barrier $E_B = 36 \pm 5$ K, which is comparable with the activation energy E_A obtained from macroscopic resistance relaxation measurements²⁰.

Having established the existence of quantum domain reconfiguration dynamics at low temperatures, we proceed with setting up a closely matching open quantum system simulation on a

quantum annealer²⁸. We begin with the classical 2D interaction Hamiltonian which describes the domain states in equilibrium^{17,18}:

$$H_{int} = \frac{1}{2} \sum_{i,j}^N V(i,j)(q_i - \bar{q})(q_j - \bar{q}) - \mu \sum_i^N q_i, \quad (1)$$

where $V(i,j) = \frac{V_0 \exp(-\frac{r_{i,j}}{r_s})}{r_{i,j}}$, r_s is the screening radius, $r_{i,j} = r_i - r_j$, r_i is the i -th out of N lattice sites, q_i is the occupation number of lattice site i , the sum runs over all lattice sites and $\bar{q} = \frac{\sum_i^N q_i}{N}$. \bar{q} is the magnitude of the charge of each lattice site and the number of electrons in the system is varied by the chemical potential μ . The polarons are considered as screened point charges that can only reside on Ta sites of the triangular atomic lattice (Fig. 1a).

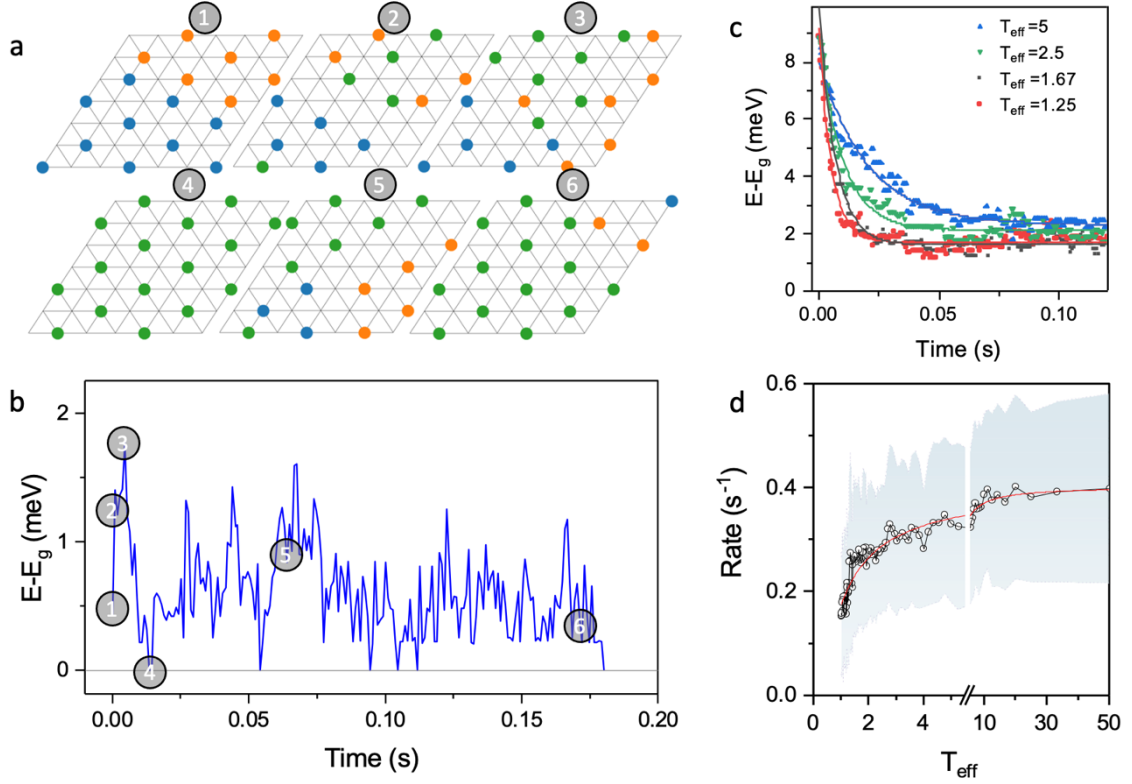


Figure 2. Simulated configurations measured at different times, the corresponding system energy, and the temperature dependence of the reconfiguration rate R . a) The initial 2-domain state configuration with a domain wall ①. The system traverses the energy landscape through multiple multi-qubit tunneling events ② and ③, to the ground state ④. Thereafter, the system is spontaneously excited, showing other domain configurations, such as ⑤ and ⑥. The excitation is thought to be the result of some external excitation such as cosmic rays²⁹. b) Energy difference between measured configurations and the ground state versus time. The horizontal line emphasizes when the system is in the ground state. c) The temperature dependence of the reconfiguration rate R in the simulation.

H_{int} describes the domain structure and salient features of the phase diagram very well¹⁷, but not the quantum dynamics. To introduce quantum tunneling between different configurations of domains we first simplify H_{int} to $H'_{int} = \sum_{i,j}^N Q_{i,j} q_i q_j$, where $Q_{i,j} = \frac{1}{2}V(i,j) - \frac{1}{2N}\sum_k(V(i,k) + V(k,j)) + \frac{1}{2N^2}\sum_{k,l}V(k,l) - \mu\delta_{i,j}$. This makes (1) applicable to the quadratic unconstrained binary optimization formalism implemented on the D-Wave ‘Advantage’ quantum processor, with 5436 physical qubits. The Hamiltonian that is simulated is the form of the transverse field Ising model (TFIM):

$$H = -\frac{A(t)}{2}\sum_i \sigma_i^x + \frac{B(t)}{2}\left(\sum_{i < j} J_{i,j} \sigma_i^z \sigma_j^z + \sum_i h_i \sigma_i^z\right), \quad (2)$$

where $\sigma_i^{x,z}$ are Pauli matrices operating on a qubit q_i , $J_{i,j}$ are couplings between qubits q_i and q_j and h_i are the longitudinal external fields at q_i . In order to map H'_{int} onto H we need to apply the transformation from spin to qubit variables $\sigma_i^z = 2q_i - 1$ and by setting $h_i = \sum_{j=i}^N \frac{Q_{i,j}}{2}$ and $J_{i,j} = \frac{Q_{i,j}}{4}$, which reduces H'_{int} to the second term of (2). The σ^x term in (2) describes tunneling between different configurational states. With this additional term, our problem is mapped onto a two-dimensional TFIM.

By analogy with the dynamics of the STM experiment, we introduce quantum dynamics with a ‘reverse annealing’ protocol, where we define the time-evolution of the Hamiltonian (2) by specifying functions for $A(t)$ and $B(t)$. The parameter t has a range of $[0, t_a]$, and plays the role of time, where t_a is the annealing time ($< 2000 \mu\text{s}$). At $t = 0$ we set $A(0) = 0$ and $B(0)$ to its maximum value, and initialize all the logical qubits to some initial state, which corresponds to a particular, non-equilibrium domain configuration. Since H at time $t = 0$ is diagonal in the number basis q_i , we are initially in the classical regime. We then turn on the transverse field $A(t)$ to a fraction of the magnitude of $B(0)$ in a controlled manner. The maximum values of $A(t)$ and $B(t)$ are $\sim 10 \text{ h GHz}$, where h is Planck’s constant and the annealing schedule can be found here²⁹. During the reverse annealing process H is no longer diagonal in the q_i basis, and the system is in a superposition state of many configurations. Tunneling processes are now allowed between different configurations as well as quantum transitions between different states. At the end of the quantum anneal we bring H back to the classical regime $A(t_a) = 0$ ²⁸ and measure the configuration, as a direct analogy to opening the box in a Schrödinger’s cat experiment. The result is shown in Fig. 2a and b. As such, the calculation is directly analogous to the procedure followed in the STM experiments (Fig. 1e and f), with remarkably similar jumpy dynamics.

To simulate the temperature dependence of the STM quantum dynamics in Fig. 1i) we can vary the effective temperature of the system. The physical temperature of the quantum processing unit in

the D-Wave machine is fixed to $15.8 \pm 0.5 \text{ mK}$. However, by scaling $H_{int} \rightarrow H_{int}/T_{eff}$, we can scale the energy scale of H_{int} to represent the real-world temperature scale³⁰. To compare our simulations with the STM experiment, in Fig. 2d we show the reconfiguration of the domain state measured over a range $1 < T_{eff} < 50$ (unitless). The shaded area represents the error, as a standard deviation of the rate in the calculation, averaged over 8 independent runs. The quantum simulation shows remarkably similar T-dependence as the STM experiment in Fig. 1i). Fitting the rate $R(T)$ in the same way as in the experiment, we obtain an empirical scaling of the barrier energy between experiment and simulation $\frac{E_B^{STM}}{E_B^S} \simeq 27 \text{ K}$. The dynamics are quantum at all times: the Hamiltonian is the only driver able to propagate the system through the configurational energy landscape in time. However, note that in both the simulation and the experiment, the *measured* states are classical. One could argue that classical temperature effects are enough to account for all the changes in qubit values when the system is let to evolve in time. However, we find that for any value of T_{eff} the system exhibits qubit changes only when a substantial transverse field is applied during a reverse anneal ($s_{min} < 0.6$). Otherwise, none of the qubits change values. (An extensive analysis of the effect of temperature, dependence on various parameters, as well as adiabatic and diabatic processes is presented in the SI.)

To investigate the quantum equilibration process, we set up an initial configuration corresponding to a highly excited state, with all sites occupied, and measure the reconfiguration processes in time. In the simulation we manipulate the relaxation rate by varying the reverse annealing protocol to control the amount of phase space available to the system at a given time from almost zero to the entire phase space. The system can thus in principle be scaled in size to the experimental scale of hundreds of qubits, which would reproduce the timescale of the reconfiguration process to match the experiment. A typical measurement showing how the system relaxes is shown in Fig 2c, showing direct correspondence with the STM reconfiguration timeline (Figs. 1f and g). The steps in the time-evolution (Fig. 1f and 2b) imply a remarkably similar susceptibility of the quantum processes to external disturbances in both cases.

Calculations show that a substantial transverse field is required to initiate dynamics. While this is far from maximum ($s_{min} = 0$), we are able to tune the relaxation rate through all the available timescales with $0 < s_{min} < 0.6$, which suggests that entanglement between different configurational states is the main driver of dynamics. $s_{min} \sim 0.6$ appears to be the cut-off point beyond which the overlap between states is too small to observe tunneling on relevant timescales. With $s_{min} < 0.6$ we are able to tune the overlap so that the available phase space for tunneling covers everything from zero to all possible states. The connection between the microscopic quantum dynamics in Fig. 2 and the tunneling processes in the energy landscape Fig. 1f suggested by experiments now becomes clear

from the simulation. One difference between the two realizations should be noticed: In simulations, the average number of particles is kept constant by adjusting μ . In the experiment, the number of electrons may change because of charge injection through the tip or via dissipation into the bulk of the crystal. The parallel simulation and real-world experiment of quantum domain melting demonstrates the remarkable value of quantum simulations for modelling the dynamics of emergent spatial inhomogeneity in a wide variety of open quantum systems – including quantum materials such as the quantum paraelectric SrTiO_3 ⁶, high temperature superconductors such as $\text{Bi}_2\text{Sr}_2\text{CaCu}_2\text{O}_{8+x}$ ³¹, and tunneling between false vacuum states in the early inflationary cosmological energy landscape^{5,32,33} amongst others. We end by noting that the presented quantum simulation of a realistic system, such as the one presented, would not be possible with a current state of the art conventional computer.

Acknowledgments

We wish to acknowledge discussions with Tomaž Prosen, Marko Žnidarič and Tomaž Mertelj. Single crystals were grown for this work by Petra Sutar, funding from ARRS project P-0040, N1-0092 and young researcher grants, P17589 and P08333. This project has received funding from the European Union's Horizon 2020 research and innovation program under the Marie Skłodowska-Curie grant agreement No 701647.

References

1. Pitaevskii, L. P. & Lifshitz, E. M. *Physical Kinetics: Volume 10 (Course of Theoretical Physics)*. (Butterworth-Heinemann, 1981).
2. Baldan, A. Review Progress in Ostwald ripening theories and their applications to nickel-base superalloys Part I: Ostwald ripening theories. *Journal of Materials Science* **37**, 2171–2202 (2002).
3. Turner, M. S. & Wilczek, F. Is our vacuum metastable? *Nature* **298**, 633–634 (1982).
4. Roberts, B. M. *et al.* Search for domain wall dark matter with atomic clocks on board global positioning system satellites. *Nature Communications* **8**, 1195 (2017).
5. Coleman, S. Fate of the false vacuum: Semiclassical theory. *Phys Rev D* **15**, 2929–2936 (1977).
6. Kustov, S., Liubimova, I. & Salje, E. K. H. Domain Dynamics in Quantum-Paraelectric SrTiO_3 . *Physical Review Letters* **124**, (2020).

7. Thomas, L. *et al.* Macroscopic quantum tunnelling of magnetization in a single crystal of nanomagnets. *Nature* **383**, 145–147 (1996).

8. Chudnovsky, E. M. & Tejada, J. *Macroscopic Quantum Tunneling of the Magnetic Moment*. (Cambridge University Press, 1998). doi:10.1017/cbo9780511524219.009.

9. Kandala, A. *et al.* Hardware-efficient variational quantum eigensolver for small molecules and quantum magnets. *Nature* **549**, 242–246 (2017).

10. Awschalom, D. D., Smyth, J. F., Grinstein, G., DiVincenzo, D. P. & Loss, D. Macroscopic quantum tunneling in magnetic proteins. *Phys Rev Lett* **68**, 3092–3095 (1992).

11. Feynman, R. P. Simulating physics with computers. *Int J Theor Phys* **21**, 467–488 (1982).

12. King, A. D. *et al.* Scaling advantage over path-integral Monte Carlo in quantum simulation of geometrically frustrated magnets. *Nat Commun* **12**, 1113 (2021).

13. Lifshitz & Yu., K. Quantum kinetics of phase transitions at temperatures close to absolute zero. *Sov. Phys. JETP* **35**, 206 (1972).

14. IAEA. Livechart - Table of Nuclides - Nuclear structure and decay data.pdf. *Table of Nuclides - Nuclear structure and decay data* <https://www-nds.iaea.org/relnsd/vcharthtml/VChartHTML.html> (2020).

15. Blatter, G., Feigel'man, M. V., Geshkenbein, V. B., Larkin, A. I. & Vinokur, V. M. Vortices in high-temperature superconductors. *Rev Mod Phys* **66**, 1125–1388 (1994).

16. Shukla, K., Chen, P.-S., Chen, J.-R., Chang, Y.-H. & Liu, Y.-W. Macroscopic matter wave quantum tunnelling. *Communications Physics* **3**, (2020).

17. Vodeb, J. *et al.* Configurational electronic states in layered transition metal dichalcogenides. *New J Phys* **21**, 083001 (2019).

18. Karpov, P. & Brazovskii, S. Modeling of networks and globules of charged domain walls observed in pump and pulse induced states. *Scientific Reports* **8**, 1–7 (2018).

19. Stojchevska, L. *et al.* Ultrafast Switching to a Stable Hidden Quantum State in an Electronic Crystal. *Science* **344**, 177–180 (2014).

20. Vaskivskyi, I. *et al.* Controlling the metal-to-insulator relaxation of the metastable hidden quantum state in 1T-TaS₂. *Science* **1**, e1500168 (2015).

21. Ma, L. *et al.* A metallic mosaic phase and the origin of Mott-insulating state in 1T-TaS₂. *Nature Communications* **7**, 1–8 (2016).

22. Cho, D. *et al.* Nanoscale manipulation of the Mott insulating state coupled to charge order in 1T-TaS₂. *Nature Communications* **7**, 10453 (2016).

23. Vaskivskyi, I. *et al.* Fast electronic resistance switching involving hidden charge density wave states. *Nature Communications* **7**, 11442 (2016).

24. Qiao, S. *et al.* Mottness Collapse in 1T-TaS₂-xSex Transition-Metal Dichalcogenide: An Interplay between Localized and Itinerant Orbitals. *Physical Review X* **7**, 041054 (2017).

25. Gerasimenko, Y. A., Karpov, P., Vaskivskyi, I., Brazovskii, S. & Mihailovic, D. Intertwined chiral charge orders and topological stabilization of the light-induced state of a prototypical transition metal dichalcogenide. *npj Quantum Materials* **4**, 1–9 (2019).

26. Laulh  , C. *et al.* Ultrafast Formation of a Charge Density Wave State in 1T-TaS₂: Observation at Nanometer Scales Using Time-Resolved X-Ray Diffraction. *Physical Review Letters* **118**, 247401 (2017).

27. Elliott, S. R. A.c. conduction in amorphous chalcogenide and pnictide semiconductors. *Adv. Phys.* **36**, 135–218 (1987).

28. King, A. D. *et al.* Observation of topological phenomena in a programmable lattice of 1,800 qubits. *Nature* **560**, 456–460 (2018).

29. Hanington, F. QPU-Specific Anneal Schedules – D-Wave Systems. *QPU-Specific Anneal Schedules – D-Wave Systems* <https://support.dwavesys.com/hc/en-us/articles/360005267253-QPU-Specific-Anneal-Schedules> (2021).

30. Albash, T., Vinci, W., Mishra, A., Warburton, P. A. & Lidar, D. A. Consistency tests of classical and quantum models for a quantum annealer. *Phys Rev A* **91**, 042314 (2015).

31. Yu, Y. *et al.* High-temperature superconductivity in monolayer Bi₂Sr₂CaCu₂O_{8+  }. *Nature* **575**, 156–163 (2019).

32. Linde, A. *Inflationary Cosmology*. (Springer, 2008). doi:10.1007/978-3-540-74353-8.
33. Ng, K. L., Opanchuk, B., Thenabadu, M., Reid, M. & Drummond, P. D. The fate of the false vacuum: Finite temperature, entropy and topological phase in quantum simulations of the early universe. *Arxiv* (2020).